Journal of Catalysis **184,** 440–454 (1999)
Article ID jcat.1999.2459, available online at http://www.idealibrary.com on IDEAL®

Characterization of SnO_2/Al_2O_3 Lean NO_x Catalysts

P. W. Park,[1] H. H. Kung, D.-W. Kim,[2] and M. C. Kung[3]

Department of Chemical Engineering, Northwestern University, Evanston, Illinois 60208-3120

Received October 29, 1998; revised February 18, 1999; accepted February 18, 1999

SnO_2/Al_2O_3 prepared with $SnCl_2$ impregnation onto sol–gel Al_2O_3 and calcined at 800°C is one of the most active catalysts for lean NO_x reduction with propene under high partial pressures of O_2 (15%) and H_2O (10%) and space velocity (30,000 h^{-1}). An unusual feature of this catalyst is the independence of maximum NO conversion over a wide range of Sn contents (1 to 10 wt% Sn). This catalyst is, however, sensitive to other preparation variables such as the nature of Sn precursor and the calcination temperature. X-ray photoelectron spectroscopic results indicate that Sn is present in the +4 oxidation state irrespective of Sn loadings. X-ray diffraction, temperature-programmed desorption, and temperature-programmed reduction results indicate a wide range of oxo–tin cluster sizes as well as different ratios of amorphous and crystalline SnO_2 present in samples with different Sn loadings. The Sn(IV) in the amorphous SnO_2 fraction can be reduced to Sn(II) below 450°C in the TPR experiments. In fact, all of the SnO_2/Al_2O_3 catalysts have very similar H_2 uptake features below 450°C. In view of the fact that they also have very similar catalytic properties, it appears likely that easily reducible amorphous SnO_2 is an active phase for lean NO_x catalysis in these samples.

I. INTRODUCTION

Selective catalytic reduction of NO_x in the presence of excess oxygen and water is a challenging chemical problem. In addition, the requirement of hydrothermal stability makes the formulation of a practical catalyst even more formidable. Alumina-based catalysts are attractive candidates because they are generally more stable than zeolitic materials.

Alumina reacts with many base metal oxides to form low surface area aluminates, which are sometimes inactive and impact negatively on the overall lean NO_x process (1). SnO_2 does not form any known compounds with alumina. Moreover, bulk SnO_2 is a good lean NO_x catalyst at low space velocities and in a feed with a relatively low O_2/C_2H_4 ratio of 10 (2). Thus, SnO_2/Al_2O_3 is a candidate for lean NO_x catalysis. In our preliminary report, we have shown that SnO_2/Al_2O_3 catalyzes the selective reduction of NO_x by C_3H_6 (3). The catalyst, prepared by introduction of $SnCl_2$ precursor via incipient wetness onto a γ-Al_2O_3 prepared by the sol–gel method, is among the most active and selective alumina based lean NO_x catalyst known to date (3). This catalyst is also stable under hydrothermal conditions (3). Interestingly, SnO_2/Al_2O_3 catalysts, prepared with different methods by other investigators and evaluated under similar feed composition but at *significantly lower space velocities*, have somewhat lower N_2 yields than our catalysts (4, 5). In addition, Sn-ZSM-5 is a very poor lean NO_x catalyst unless it is mixed physically with Mn_2O_3 (6). Thus, in order to make further advances, an understanding of the active site requirement of SnO_2 based catalysts appears to be necessary.

In many of the better lean NO_x catalysts, the active site appears to consist of highly dispersed metal or metal oxide clusters (1, 7–9). Thus, a major focus of this study is to investigate the catalytic performance of oxo–tin species of different cluster sizes. Dispersion of SnO_2 on alumina was varied by changing the Sn loading, the nature of Sn precursor, the method of Sn introduction and the calcination temperature. XRD (X-ray diffraction), TPR (temperature-programmed reduction), TPD (temperature-programmed desorption), and XPS (X-ray photoelectron spectroscopy) were used to probe the properties of SnO_2 clusters on alumina.

The catalysts were evaluated according to their activities and their competitiveness factors. Lean NO_x catalysis can be viewed as a process in which two oxidants, NO_x and O_2, compete for a limited concentration of hydrocarbon reductants (Eqs. [1] and [2]). The competitiveness factor, defined as the ratio of the rate of Eq. [1] to the sum of the rates of Eqs. [1] and [2], indicates the efficiency of a catalyst for NO_x reduction. A typical feature of the catalytic performance of many lean NO_x catalysts is the existence of a temperature (T_{max}) of maximum NO conversion. This temperature often occurs when hydrocarbon conversion is close to or at completion. In this paper, a catalyst is labeled as *active* when the temperature of maximum NO_x conversion is low and is regarded as *competitive* when the maximum NO conversion

[1] Current address: Caterpillar Inc., Technical Center E., Mossville, IL 61552.
[2] On leave from Korea Electric Power Research Institute.
[3] To whom correspondence should be addressed.

0021-9517/99 $30.00

is high. It has also been generally observed that over many lean NO_x catalysts, NO_2 is the actual oxidant that reacts with the hydrocarbon (10–15). Thus, our investigation also evaluates different SnO_2/Al_2O_3 catalysts with respect to their ability to catalyze the oxidation of NO to NO_2 (Eq. [3]).

$$((12+y)/x)NO_x + 2C_3H_6 \rightleftharpoons ((12+y)/2x)N_2 + 6H_2O + yCO_2 + (6-y)CO, \quad [1]$$

$$3(1+x)/2O_2 + C_3H_6 \rightleftharpoons 3CO_x + 3H_2O, \quad [2]$$

$$NO + 1/2O_2 \rightleftharpoons NO_2. \quad [3]$$

II. EXPERIMENTAL

II.A. Catalyst Preparation

The SnO_2/Al_2O_3 catalysts were prepared by incipient wetness impregnation with an ethanol solution of $SnCl_2$ (Aldrich, 99.99+%) on γ-alumina (surface area = 240 m^2/g, pore volume = 1.4 mL/g). γ-Al_2O_3 was prepared by hydrolysis of aluminum isopropoxide (99.99+%, Aldrich) in the presence of 2-methyl-2,4-pentanediol (99%, Aldrich) similar to the method of Maeda *et al.* (16). The impregnated sample was then calcined in 100 mL/min flowing air at a temperature ramp of 1°C/min until 700°C and maintained at 700°C for 2 h. At 500°C, 2% H_2O was added to the air stream, and at 700°C, 6% H_2O was added. The concentration of the $SnCl_2$ solution was adjusted so as to yield the desired Sn loadings in the final catalysts. The tin content was varied from 1 to 15 wt% based on Sn. The catalysts were designated by Sn*y*, where *y* denotes the nominal tin loading (wt%). The actual Sn loadings (Table 2) were usually lower than the nominal values due to the fact that some $SnCl_2$ evaporated during high-temperature calcination.

For comparison, additional supported Sn catalysts were prepared by impregnating different Sn precursors. The Sn-Ac-5 catalyst was a 5 wt% Sn catalyst prepared using a Sn(II) acetate precursor (Aldrich), and the Sn-IP-10 catalyst was a 10 wt% Sn catalyst prepared with Sn(IV) isopropoxide (Alfa Aesar 98%). The impregnated samples were dried at 120°C for 24 h and then calcined either to 500°C for 4 h or for an additional 2 h at 800°C. Sn-sol-10 was prepared by hydrolysis of Sn isopropoxide and Al isopropoxide dissolved in 2-methyl-2,4-pentanediol. It was calcined in the same way as the γ-alumina carrier preparation. The unsupported SnO_2 standard (99.9%) was obtained from Aldrich Inc.

II.B. Catalytic Reactions

The catalytic reaction was performed in a fused silica microreactor, and, unless specified, in a feed of 15% O_2, 10% H_2O, 0.1% NO, and 0.1% propene, with the balance being He. The total flow rate was 200 ml/min and 0.2 g of catalyst was used, which corresponded to a space velocity of 30,000 h^{-1}. The reaction products were analyzed by gas chromatography as described earlier (1). Both CO and CO_2 were observed for the reaction of C_3H_6. NO_x conversion was determined by the N_2 produced. No N_2O was detected. Thus, the N_2 yield equaled the NO conversion. For the 800°C calcined samples, the catalysts were pretreated in the reaction feed at 600°C for 2 h before actual data were recorded. For reasons not yet understood, there was a 5–20% improvement in the N_2 yield after this pretreatment than without it. In the selective reduction experiment where the effect of NO_2 was examined, all the catalysts were first used in the NO reduction experiment and then used in the NO_2 experiment. In some cases, the exit gas from the reactor was analyzed by a NO_x analyzer to determine the relative ratio of NO to NO_2.

II.C. Temperature-Programmed Reduction (TPR) and Desorption (TPD)

Desorbed species in TPD of NO from SnO_2/Al_2O_3 catalysts were detected with a quadrupole mass spectrometer (UTI 100 C). Prior to the TPD experiment, 0.1 g of the catalyst was heated to 500°C in 100 cc/min flow of 20% O_2/He at a ramp rate of 16°C/min. It was maintained at that temperature for 30 min and then quench cooled to room temperature in O_2. The sample was purged in He (UHP He, Matheson, purified further with O_2 trap) until no oxygen could be detected. ^{15}NO (100%, 15 cc/min) was introduced to the sample for 30 s at room temperature, and then the sample was purged for 40 min in a He stream. ^{15}NO was used to avoid interference from the background gases present in the TPD system. The ramping rate was 20°C/min.

II.D. Other Characterizations

BET surface area measurements were performed using an Omnisorp 360 automatic system (Omicron Technology). X-ray powder diffraction patterns were obtained with a Rigaku diffractometer using Cu $K\alpha$ radiation. Elemental analysis, by inductively coupled plasma (ICP) method, was conducted using a Thermol Jerrell-Ash Instrument. The catalysts were dissolved in 2% HF solution for analysis. XPS analysis was performed in a VG Scientific spectrometer system equipped with a magnesium anode (1253.6 eV). Binding energies for the catalyst samples were referenced to the C 1*s* line (284.6 eV) of the carbon contaminant.

III. RESULTS

III.A. Catalytic Dependence on Tin Loading

Figure 1a compares the N_2 yield and Fig. 1b compares the integral N_2 production rate for NO_x reduction over SnO_2/Al_2O_3 catalysts (800°C calcined) with different Sn loadings in a feed of 0.1% NO, 0.1% C_3H_6, 15% O_2, and

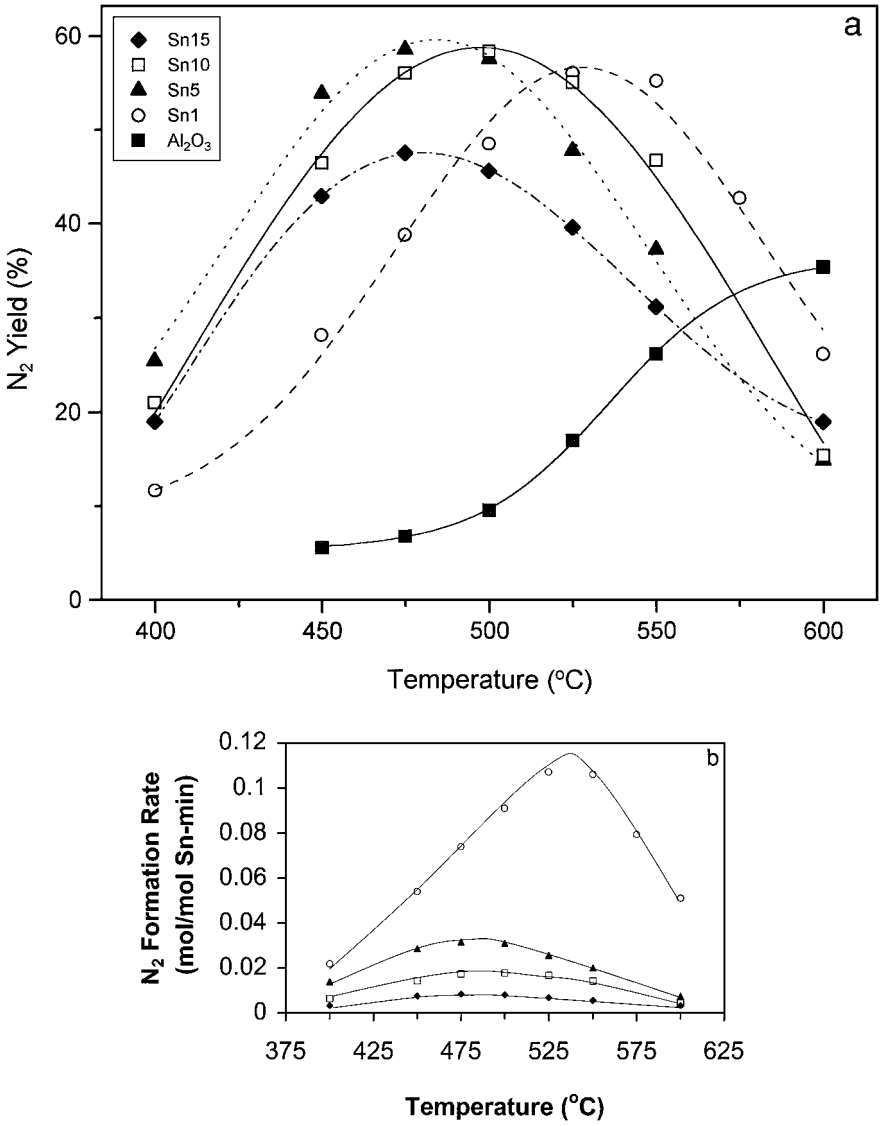

FIG. 1. The effect of Sn loading on (a) the N_2 yield and (b) the integral N_2 formation rate per mole of Sn in the selective reduction of NO over SnO_2/Al_2O_3 catalysts (0.1% NO, 0.1% C_3H_6, 15% O_2, 10% H_2O, SV = 30,000 h^{-1}). Fig. 1a is taken from Ref. (3).

10% H_2O and an SV of 30,000 h^{-1}. The catalysts were very active, and the highest observed rate was 2.4×10^{-5} mol/min-g cat, corresponding to 60% NO conversion. The N_2 yields, at the temperature of maximum NO conversion (Fig. 1a) were very similar for the Sn1, Sn5, and Sn10 catalysts. The only difference was the temperature of maximum NO conversion which was significantly higher for Sn1. However, the performance of the Sn15 sample was poorer. On the basis of per mole of Sn, the activity decreased with increasing Sn loading (Fig. 1b) because of decreasing SnO_2 dispersion.

For the Sn1, Sn5, and Sn10 catalysts, a similar lack of dependence of N_2 yields on Sn loading was observed when NO was replaced with NO_2 in the feed (Fig. 2a). In fact, the catalytic performances of all three catalysts converged with NO_2 in the feed due to the large improvement in the activity of Sn1 catalyst and the indifference of the other two catalysts (Sn5 and Sn10) to the nature of NO_x in the feed. Again, the integral rate per mole of Sn decreased with increasing SnO_2 loading (Fig. 2b). Table 1 compares the relative concentrations of NO and NO_2 in the exit gas of Sn1 and Sn10 catalyst for the selective reduction of NO_2. Although the concentrations of NO_2 at the lower temperatures were non-negligible, they were below the equilibrium values at all temperatures. In all events, supported Sn catalysts are not as active as Cu-based catalysts in promoting the reduction of NO_2 to NO (17, 18).

Figure 3 compares the C_3H_6 consumption rate and conversion over the Sn1, Sn5, and Sn10 catalysts with different oxidants: O_2, NO + O_2, and NO_2 + O_2. For all three catalysts,

TABLE 1

Composition of NO_x and NO_2 Conversions in the Selective Reduction of NO_2 by C_3H_6 (0.1% NO_2, 0.1% C_3H_6, 15% O_2, 10% H_2O, SV = 30,000 h^{-1})

Temp. (°C)	Equilibrium composition		Sn1			Sn10		
			NO_2 conversion to N_2 (%)	Exit composition		NO_2 conversion to N_2 (%)	Exit composition	
	NO (%)	NO_2 (%)		NO (%)	NO_2 (%)		NO (%)	NO_2 (%)
400	42.5	57.5	22.4	59.3	40.7	34.9	53.6	46.4
450	60.1	39.9	44.3	80.4	19.6	65.5	88.7	11.3
500	73.7	26.3	70.1	90.4	9.6	65.5	97.2	2.8
550	82.9	17.1	66.9	90.3	9.7	46.5	93.5	6.5

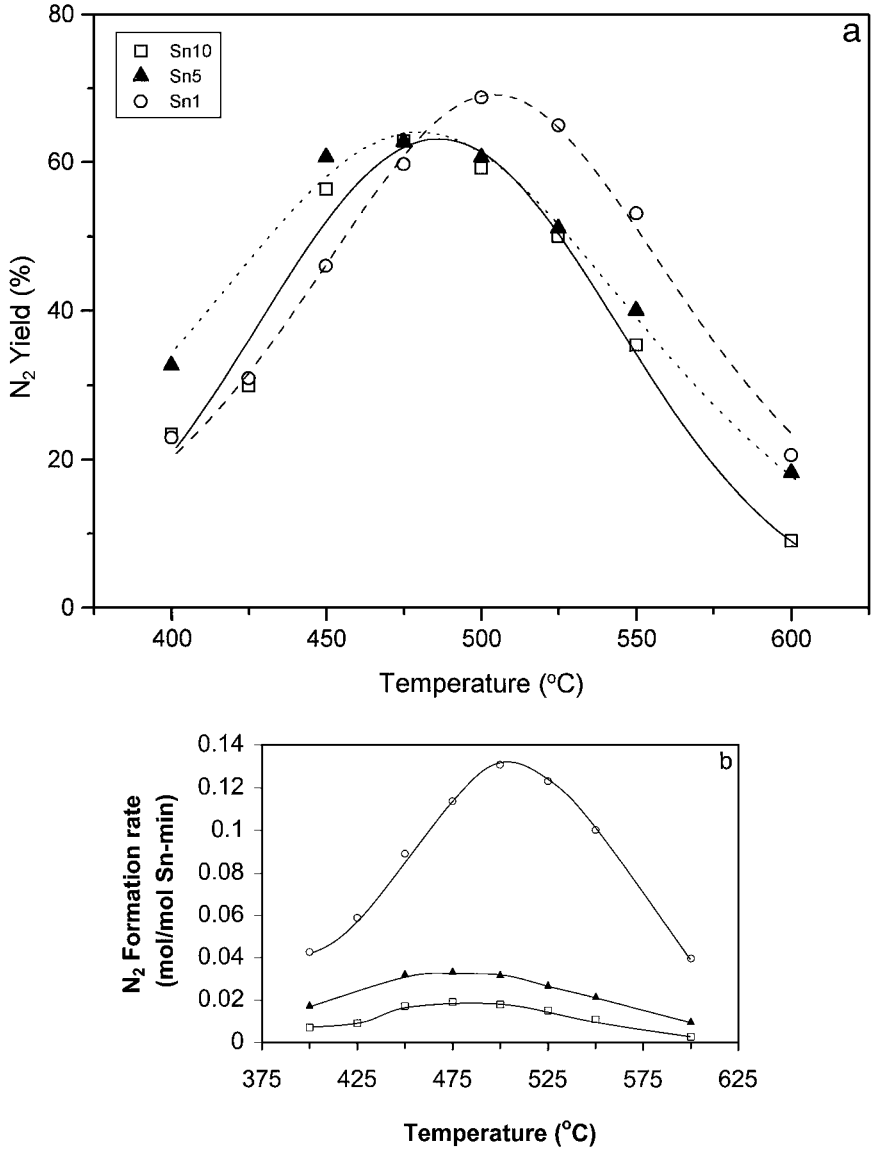

FIG. 2. The effect of Sn loading on (a) the N_2 yield and (b) the integral N_2 formation rate per mole of Sn in the selective reduction of NO_2 over SnO_2/Al_2O_3 catalysts (0.1% NO_2, 0.1% C_3H_6, 15% O_2, 10% H_2O, SV = 30,000 h^{-1}).

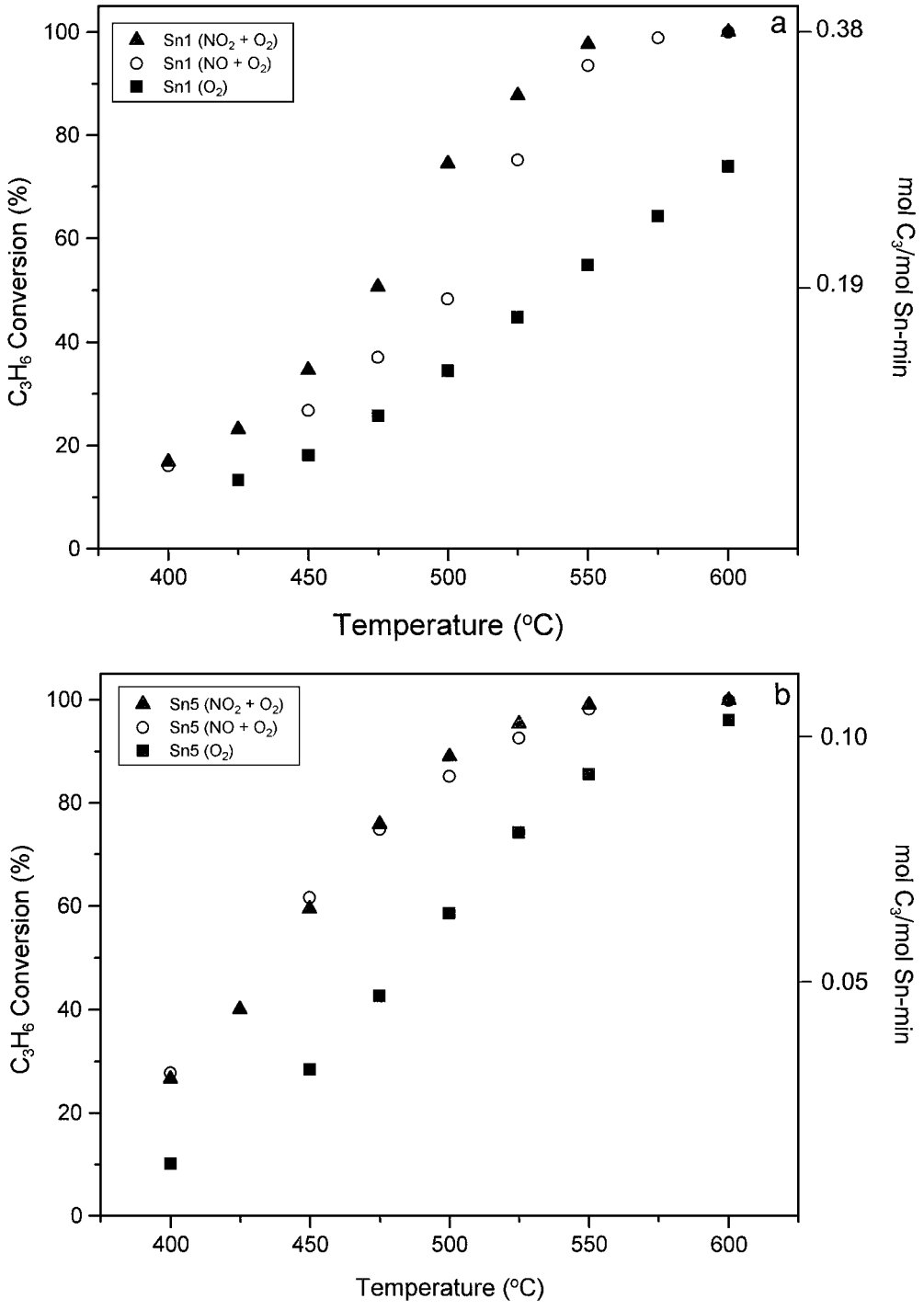

FIG. 3. The effect of oxidant in the feed on the C_3H_6 conversion and integral rate of reaction over SnO_2/Al_2O_3 catalysts (0.1% NO or NO_2, 0.1% C_3H_6, 15% O_2, 10% H_2O, SV = 30,000 h^{-1}). (a) Sn1, (b) Sn5, (c) Sn10.

the conversion of C_3H_6 was high when NO_x was present. NO_2 was more effective than NO in enhancing the hydrocarbon conversion for Sn1 catalyst, but the difference was small for Sn5 and Sn10 catalysts. Thus, it appears that the higher Sn loading catalysts may be very efficient in the oxidation of NO to NO_2. NO oxidation reaction was examined over Sn1 and Sn10 with a feed of 0.1% NO, 5% O_2, and an SV of 30,000 h^{-1} (Fig. 4). The NO oxidation activity increased with increasing temperature. While it was true that the Sn10 catalyst was slightly more active than the Sn1 catalyst in the oxidation of NO, the NO conversions over both catalysts were very low and the NO_2 concentration

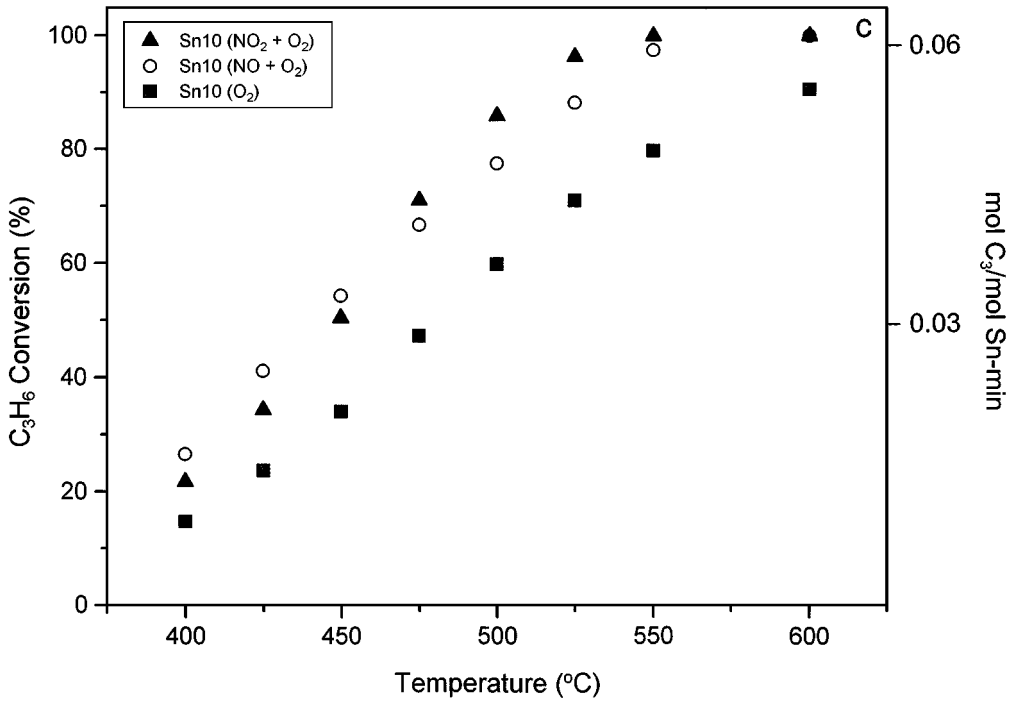

FIG. 3—*Continued*

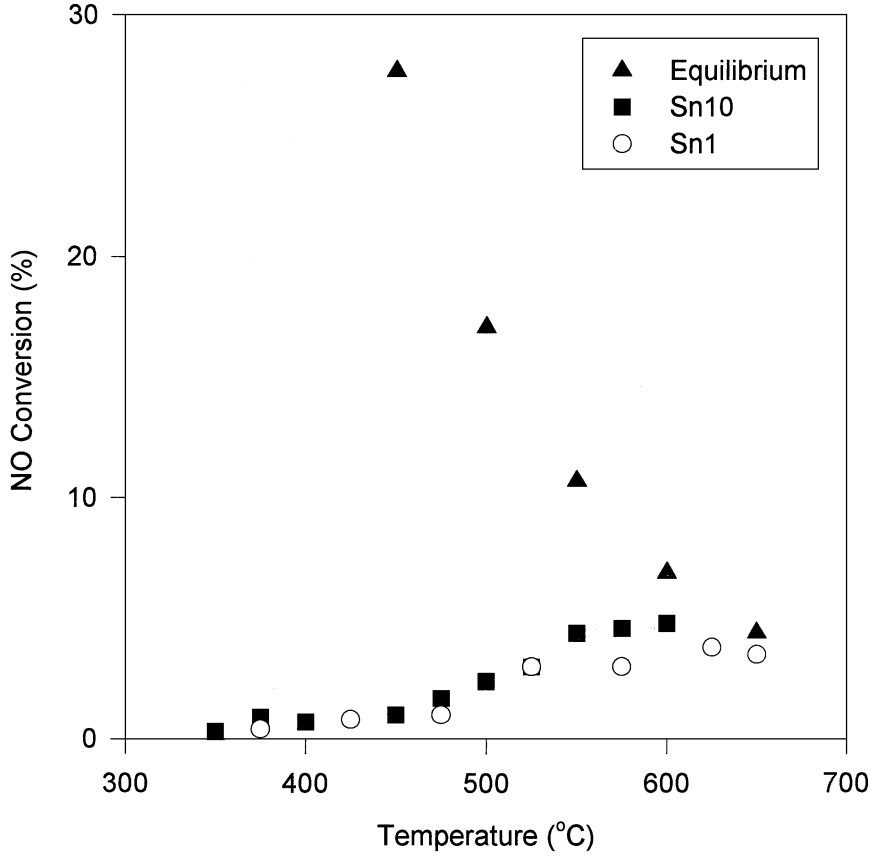

FIG. 4. The activity for NO oxidation over SnO_2/Al_2O_3 catalysts (0.1% NO, 5% O_2, SV = 30,000 h^{-1}).

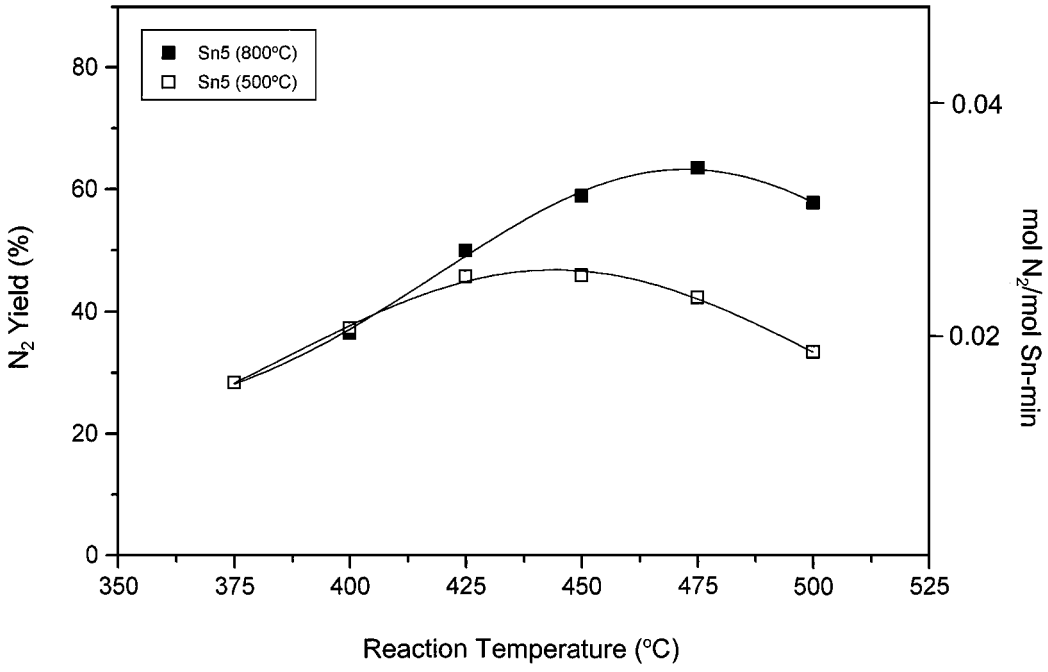

FIG. 5. The effect of calcination temperature on the N_2 yield and integral reaction rate of NO reduction over Sn5 catalyst (0.1% NO, 0.1%C_3H_6, 5% O_2, 4% H_2O, SV = 30,000 h^{-1}).

remained below the equilibrium value even at 600°C. In addition, it was found in separate experiments that the NO_2 formation was suppressed significantly by the presence of 3.8% water in the feed.

III.B. Effect of Calcination Temperature

Figure 5 compares the integral N_2 production rate and yield over a Sn5 catalyst calcined at 500 and 800°C. For comparative purposes, the catalysts were not pretreated as usual in the reaction feed at 600°C (as mentioned in the Experimental Section, such pretreatment improved the catalytic activity). The two catalysts were also compared at lower water (4%) and oxygen (5%) concentrations in the feed than in all the other experiments. It can be seen that high temperature calcination improved the N_2 yield of the catalyst when the reaction temperatures were high. Similar improvements in catalytic activities with increased calcination temperature were also observed for the Sn10 catalyst (not shown here).

III.C. Effect of Precursor and Preparative Method

Figure 6 compares the catalytic performance of SnO_2/Al_2O_3 catalysts prepared with different Sn precursors and preparation methods. It shows that Sn-Ac-5, Sn-IP-10, and Sn-sol-10 were all less competitive (lower NO_x conversion) when compared with SnO_2/Al_2O_3 catalysts prepared with $SnCl_2$ precursor.

III.D. Structural Analysis

Small but steady decreases in the specific BET surface areas accompanied the increase in tin content of the catalysts (Al_2O_3, 242 m^2/g; Sn1, 232 m^2/g; Sn5, 224 m^2/g; Sn10, 213 m^2/g; Sn15, 184 m^2/g). However, the surface areas (except for Sn15) per gram of Al_2O_3 remained invariant (about 240 m^2/g) for the different samples. This suggests that the surface areas of crystalline SnO_2 must be very small. Figure 7 shows the valence band regions in the XPS spectra of Sn1 and Sn10. Since Sn^{2+} and Sn^{4+} oxides have similar XPS Sn $3d_{5/2}$ binding energies, it is difficult to confirm the oxidation state of tin using core level spectra. However, they can be distinguished from the valence band (19, 20). The lines in the figure indicate the position of the band edges expected for SnO (Sn 5*s*-derived feature at about 2 eV) and SnO_2 (O 2*p*-derived feature at about 5 eV). The features characteristic of Sn^{4+} was observed for both samples, and Sn^{2+} species was not detected. XPS spectra also confirmed that after high temperature calcination, the surface Cl^- concentration was negligible.

Figure 8 shows the XRD pattern of Sn5 calcined at 500 and 800°C. For the 500°C calcined sample, the major features of the XRD pattern belonged to γ-Al_2O_3. The presence of a few very small peaks indicated the emergence of small SnO_2 crystallities. For the 800°C calcined sample, sharp diffraction peaks attributed to large crystallites of SnO_2 of the rutile structure were very prominent. A comparison of the XRD patterns of 800°C calcined SnO_2/Al_2O_3 catalysts with different Sn loadings is shown in Fig. 9. The

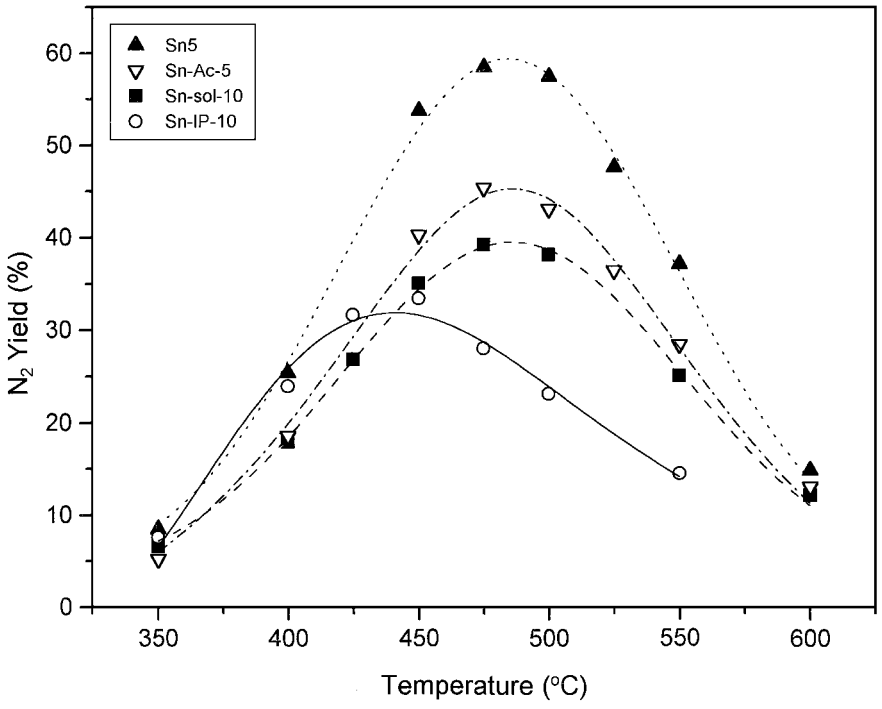

FIG. 6. The N_2 yield in the selective reduction of NO over SnO_2/Al_2O_3 catalysts prepared with different precursors (0.1% NO, 0.1% C_3H_6, 5% O_2, 4% H_2O, SV = 30,000 h^{-1}).

XRD patterns of all samples have characteristic lines of γ-Al_2O_3 and, with the exception of Sn1, peaks characteristic of SnO_2. The intensity of the SnO_2 XRD peaks and surprisingly, the full-width at half-maximum (FWHM) increased with Sn loadings. The peak broadening effect was very pronounced when the loading was increased from 10 to 15 wt%. The ratios of the areas of the diffraction peaks from the ⟨110⟩ plane of SnO_2 and ⟨400⟩ plane of Al_2O_3 are 0.22 for Sn5, 1.2 for Sn10, and 1.9 for Sn15. For Sn10 and Sn15, the area ratios of the diffraction peaks were consistent with that obtained from a physical mixture of SnO_2 and Al_2O_3 of known weights; while for Sn5, it is estimated from the ratio that 60% of the SnO_2 clusters were too small or disordered to be detected by XRD.

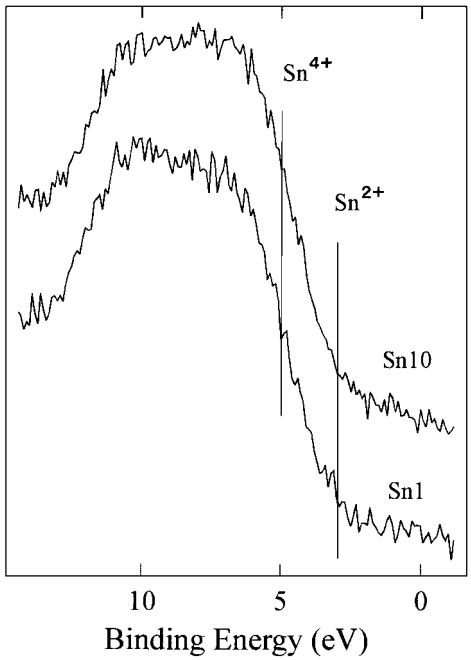

FIG. 7. XPS valence band spectra of SnO_2/Al_2O_3 catalysts.

Figures 10a and 10b show the TPR spectra for the series of 800°C calcined SnO_2/Al_2O_3 catalysts and bulk SnO_2, respectively. No detectable H_2 uptake was observed for the alumina support. There was no distinct H_2 consumption peak for Sn1 or Sn5 sample. Instead, H_2 uptake was observed starting at 100°C and continued throughout the temperature region examined. The amount of hydrogen uptake for the Sn1 sample was too small to be quantified. A high temperature, asymmetric H_2 uptake peak was observed for the Sn10 and Sn15 samples. The reduction peak temperatures of both samples were below that of the bulk SnO_2. Tables 2 shows the uptake of hydrogen molecules per Sn. For the supported catalysts, about one hydrogen was consumed per Sn atom, whereas the stoichiometry was close to 2 for bulk tin oxide. The data indicate that 97% of bulk SnO_2 can be completely reduced to Sn metal.

The XRD pattern of a Sn10 sample, after TPR and exposure to room air, showed no peaks characteristic of SnO_2

TABLE 2

ICP, H_2 Uptake in TPR, Moles Sn/g Catalyst, and % Amorphous SnO_2 for the SnO_2/Al_2O_3 Catalysts

Catalyst	ICP results	mol H_2/mol Sn	Sn/g cat. (10^{-5} mol)	% amorphous SnO_2
SnO_2	—	1.9	—	—
Sn1	1.3 wt%	Too small for accurate determination	11	100
Sn5	4.6 wt%	1.07	39	60[a]
Sn10	8.1 wt%	0.98	68	34[b]
Sn15	14.0 wt%	0.82	118	20[b]
Sn-sol-10	9.7 wt%	—	—	—
Sn-IP-10	10.2 wt%	—	—	—

[a] Estimated from XRD peak intensities.
[b] Assuming the same weight of amorphous SnO_2 per g of catalysts as in Sn5.

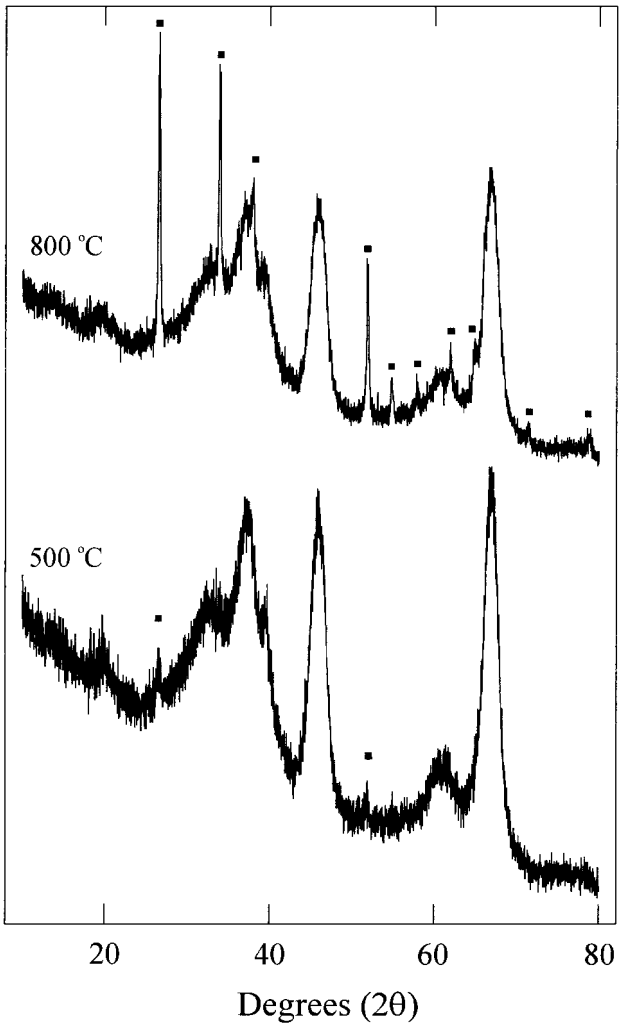

FIG. 8. XRD patterns for Sn5 catalyst at different calcination temperatures (■, SnO_2).

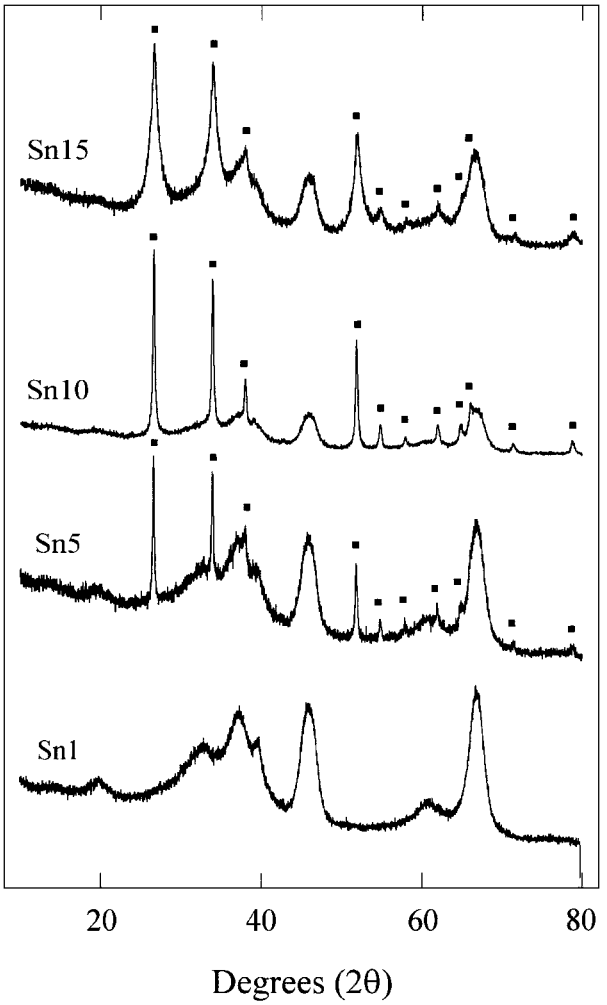

FIG. 9. XRD patterns for SnO_2/Al_2O_3 catalysts calcined at 800°C (■, SnO_2).

or SnO. After sitting 2 h in ambient atmosphere, this sample was subjected to another TPR, and the H_2 consumption was about 1/4 of the first TPR. This indicates that some re-oxidation of Sn species occurred even at room temperature (not shown here).

Temperature programmed desorption profile of ^{15}NO adsorbed on Al_2O_3 is shown in Fig. 11a. The NO desorption peak maximum was around 360°C, and a high temperature shoulder was observed at around 510°C. The other desorption products were $^{15}N_2$, $^{15}N_2O$, and O_2, the concentrations of which were very low compared with that of ^{15}NO. Whether these small amounts of $^{15}N_2$ and $^{15}N_2O$ were due to NO decomposition over Al_2O_3 or to reduction of NO by trace impurities of hydrocarbons or CO in the reaction system was not determined. Figure 11b compares the ^{15}NO desorption profile over Sn5 calcined at 500, and 800°C and that of Al_2O_3. The ^{15}NO peak for Sn5 calcined at 500°C was very much broader and shifted to a lower temperature compared with the 800°C calcined sample and

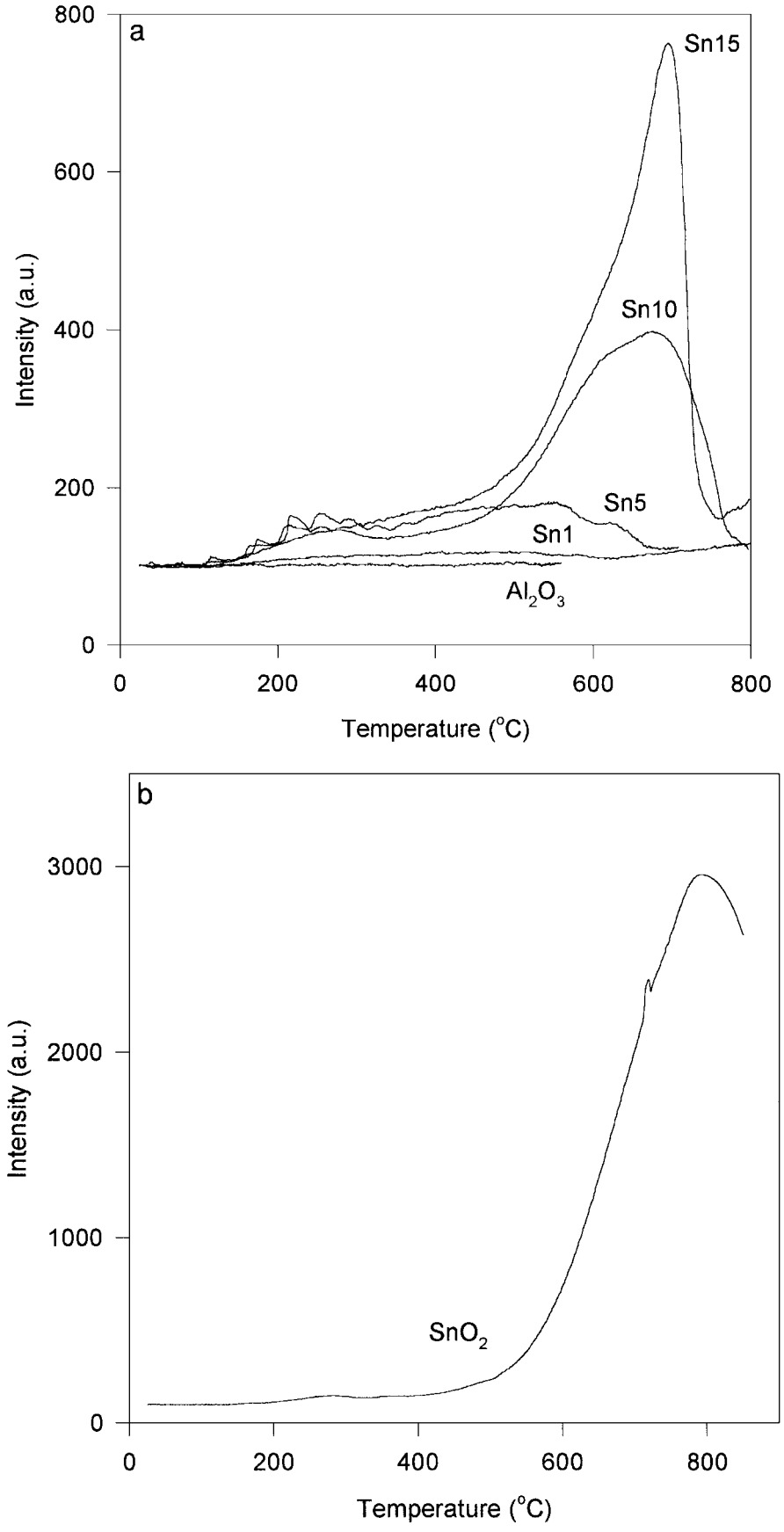

FIG. 10. TPR spectra for (a) SnO_2/Al_2O_3 catalysts and (b) SnO_2.

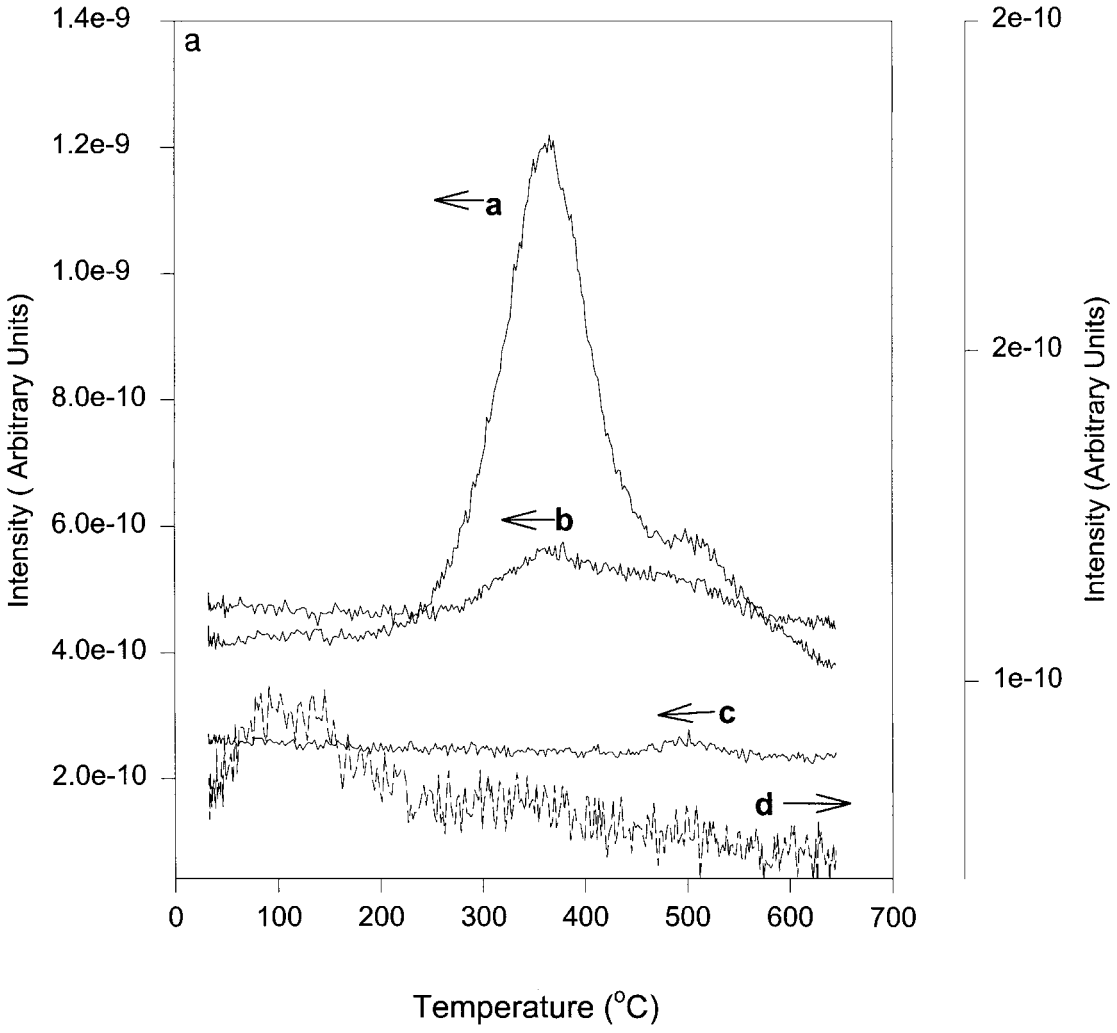

FIG. 11a. Product profile for ^{15}NO TPD spectra over Al_2O_3, (a) ^{15}NO, (b) $^{15}N_2$, (c) O_2, and (d) $^{15}N_2O$.

Al_2O_3. The latter two samples had very similar desorption profiles.

IV. DISCUSSION

The most unusual feature of the 800°C calcined SnO_2/Al_2O_3 catalysts is that the maximum NO conversions (Fig. 1a) are very similar over a wide range of Sn loadings (1–10 wt%). This is in striking contrast to the strong dependence on metal loadings exhibited by many of the lean NO_x catalysts reported in the literature. In the zeolitic systems, exchange of cations into the zeolitic channels ensures a low degree of clustering. Indeed, in over-exchanged zeolites when metal oxide is present, the maximum NO conversions almost always decreased when compared with those at a lower exchange level (21, 22). However, low overall NO_x conversions were also reported for ZSM-5 catalysts with very low ion exchange levels (23, 24). For alumina-based catalysts such as CoO_x/Al_2O_3 and AgO_x/Al_2O_3, the NO conversions decrease with increasing metal loadings (1, 7). For SnO_2/Al_2O_3, the independence of the maximum NO conversion over a wide range of Sn loadings suggests that the catalytic sites present on these catalysts have similar competitiveness factor. In other words, they show similar selectivity for reaction [1] in the overall reactions of the hydrocarbon (reactions [1] and [2]). Another unusual feature of SnO_2/Al_2O_3 catalyst is its high NO_x reduction activity. Except for Fig. 5, all reaction data were gathered at high H_2O (10%) and O_2 (15%) contents and at a high space velocity of 30,000 h^{-1}. Some of these unusual features may be understood in terms of the structure of the SnO_2 active site.

The SnO_2/Al_2O_3 catalysts with different Sn contents share some similar structural features. No Sn-alumina compound could be detected in any of the samples by XRD. All the Sn species were in the +4 oxidation state, and there were few residual Cl ions from the $SnCl_2$ precursors for all high-temperature calcined catalysts. The Sn loadings for all of the catalysts studied were below the theoretical monolayer

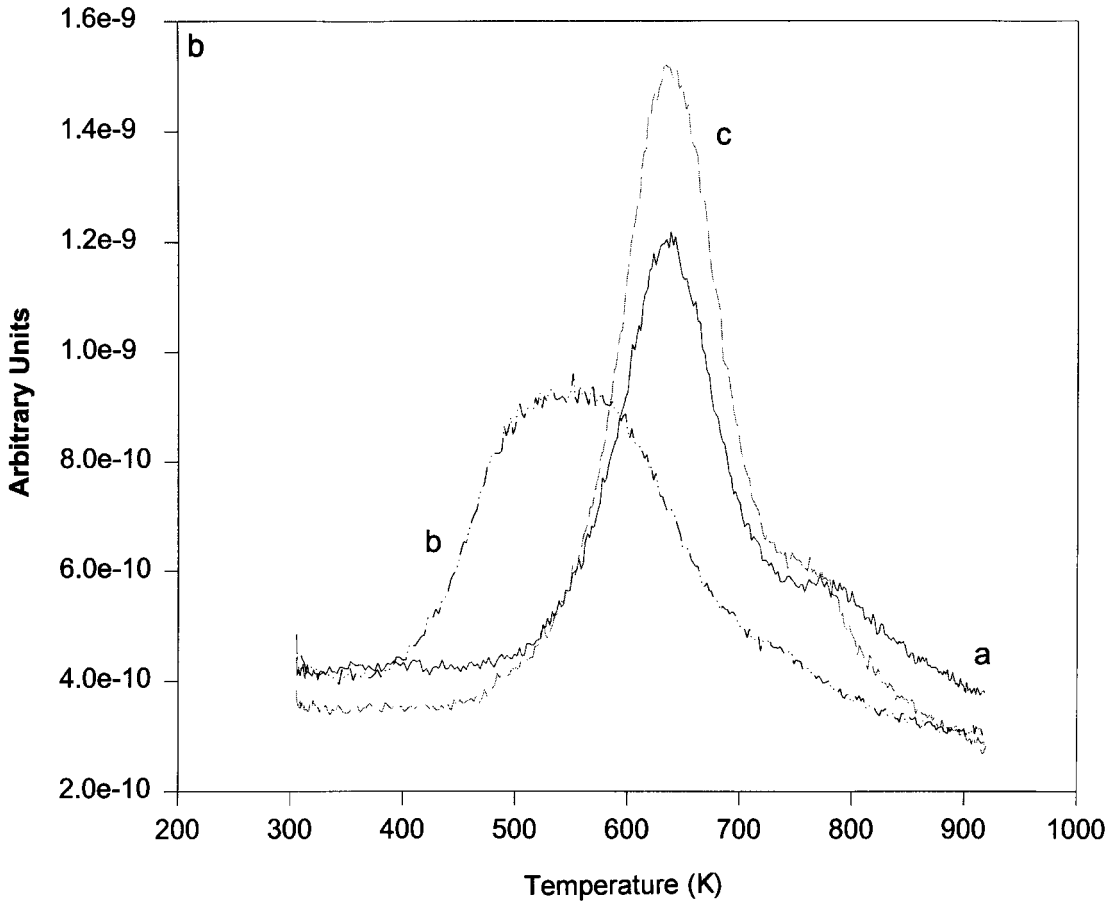

FIG. 11b. ^{15}NO desorption profile over (a) Al_2O_3, (b) Sn5 calcined at 500°C, and (c) Sn5 calcined at 800°C.

coverage of 18.4 wt% Sn (estimated by assuming that the exposed plane of SnO_2 on the support is the 110 plane). However, the distribution of the different sizes of oxo–tin clusters changes with Sn loadings and calcination temperatures as is shown by XRD, TPD, and TPR experiments.

Any crystalline SnO_2 present in Sn1 was below XRD detection limit. However, all the 800°C calcined samples with higher Sn loadings show SnO_2 XRD diffraction patterns. The ratios of crystalline to amorphous SnO_2 vary significantly with Sn loadings. Whereas most or all of the SnO_2 may be regarded as crystalline in Sn10 and Sn15 samples, only 40% are crystalline in Sn5. The crystallinity of SnO_2 in the various samples decreased with increased Sn loadings as is indicated by the full width at half maximum (FWHM) of the XRD peaks. Accompanying the significant disorder of the SnO_2 crystallites in Sn15, there is a noticeable drop in the competitiveness factor. Currently, both the phenomena of crystal disorder with increased Sn loading and the accompanying effect on the competitiveness factor are not understood and are being studied in detail.

Results of H_2 TPR experiments further clarify the nature of the oxo–tin species of the 800°C calcined samples. The continuous H_2 uptake, spanning a wide temperature range of 700°C, and the absence of a distinct peak observed for Sn1 and Sn5 (Fig. 10a) suggest a broad size distribution of the SnO_2 clusters. Below 450°C, the H_2 uptake for Sn5, Sn10, and Sn15 samples are very similar (Fig. 10a). The H_2 uptake above 450°C may be assigned to reduction of crystalline SnO_2. Indeed, for Sn5, the ratio of the H_2 uptake below and above 450°C is approximately proportional to the ratio of SnO_2 that is amorphous and crystalline as detected by XRD. For Sn10 and Sn15 samples, the presence of the large high temperature H_2 uptake peaks is also consistent with the XRD data showing that crystalline SnO_2 are the predominant species present in these samples. This assignment is also in line with the fact that bulk SnO_2 reduces at a very high temperature (800°C, Fig. 10b). Using this assignment, one can estimate the amounts of amorphous SnO_2 in theses samples and the results are summarized in Table 2. The fact, that all the samples have similar features in H_2 uptake below 450°C and similar competitiveness factors in lean NO_x catalysis, strongly suggest that the amorphous SnO_2 accounts for a significant portion of the catalytic activity. The surface area of crystalline SnO_2 in these catalysts

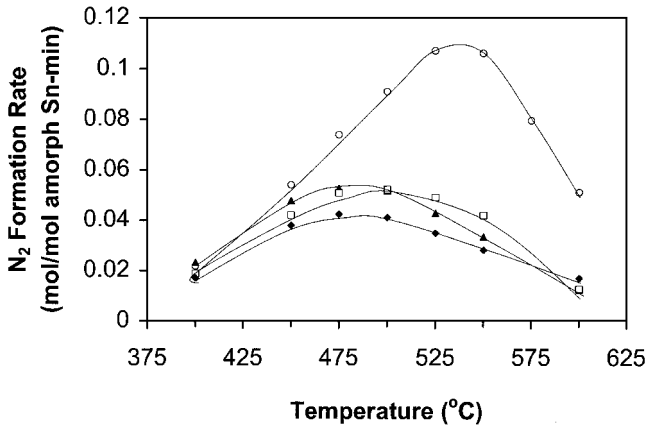

FIG. 12. The integral turnover rate of N_2 formation based on amorphous SnO_2 for Sn1, Sn5, Sn10, and Sn15 catalysts.

are probably very low as the narrow XRD peak widths suggest that they are rather large crystallites. As a result of the low surface areas, the influence of the crystalline SnO_2 on the catalytic properties of SnO_2/Al_2O_3 may be modest.

From the estimated amounts of amorphous SnO_2 in Table 2 and the data in Fig. 1, we can calculate the turnover rates for the limiting case where the active phase is the amorphous, completely dispersed SnO_2 and the contribution from crystalline SnO_2 is negligible due to their small surface areas. These are plotted in Fig. 12. Very interestingly, the turnover rates are within a factor of 2 for all the samples. These, again, are in agreement with the model that the amorphous SnO_2 contributes significantly to the catalytic properties.

The differences in the stoichiometry of H_2 uptake between the bulk SnO_2 and the supported samples are probably not due to a difference in their chemical properties. It is difficult to envision how Al_2O_3 can influence the reducibility of very large SnO_2 crystallites. Rather it is probably due to heat transfer by Al_2O_3. The reduction of Sn^{2+} to metallic Sn is kinetically slower than the corresponding reduction of Sn^{4+} to Sn^{2+}. In the reduction of bulk SnO_2, there is no dissipation by Al_2O_3 in the first step of the reduction ($SnO_2 + H_2 \rightarrow SnO + H_2O$), and the bulk SnO_2 is heated up substantially, facilitating the next step of the reduction of SnO to Sn.

The TPR results suggest that a broad spectrum of SnO_2 species, presumably of different cluster sizes, exists on SnO_2/Al_2O_3. Since the turnover rate based on amorphous SnO_2 varies little (Fig. 12) with Sn loadings, it is probable that the ability of oxo–tin species to promote selective NO reduction over combustion reaction may be independent of the cluster size over a wide range. However, when the preparative method deviates from the standard procedure of impregnating $SnCl_2$ onto Al_2O_3 and subsequent calcination at 800°C, the effectiveness of the SnO_2/Al_2O_3 for NO_x reduction decreases. The nonstandard samples include those prepared by impregnating Al_2O_3 with Sn acetate or Sn isopropoxide precursor or by co-gelling tin isopropoxide and alumina isopropoxide. The tin loadings ranged from 5 wt% for the sample prepared with acetate precursor to 10 wt% for the latter two samples. The XRD spectra of all these samples, after calcination at 800°C show only the characteristic lines of Al_2O_3. Interestingly, Sn5 prepared with $SnCl_2$ but only calcined to 500°C also has only XRD amorphous SnO_2 and poorer catalytic properties than the 800°C calcined sample. Only Sn10 calcined at 500°C has XRD detectable SnO_2 and it is a better catalyst than Sn5 calcined at 500°C.

In other words, among the Sn5 and Sn10 samples, those that contain both amorphous SnO_2 and large crystallites of SnO_2 are catalytically superior to the others that contain only amorphous SnO_2. Yet the conclusion from the comparisons among 800°C calcined samples of different Sn loadings is that amorphous SnO_2 appears to be catalytically much better for NO_x reduction than SnO_2 crystallites.

There are two possible explanations for this apparent contradiction. The absence of XRD detectable SnO_2 in the nonstandard samples suggests that the oxo–tin species are much more disperse than those samples containing crystalline SnO_2. Thus, one explanation is that below a certain critical size of oxo–tin clusters, the oxo–tin species catalyze combustion reaction and degrade the catalytic performance. Another explanation is that Al_2O_3 contributes to the reaction but could be prevented in doing so when its active centers are covered by disperse SnO_2. The effect of heat treatment is to agglomerate oxo–tin species, as evident by the appearance of crystalline SnO_2 upon heating Sn5 to 800°C. Concomitant with the agglomeration of SnO_2, Al_2O_3 surface sites previously covered by SnO_2 is re-exposed as is shown by the ^{15}NO TPD experiments (Fig. 11b). The NO desorption profile of Sn5 calcined at 500°C is significantly broader than that of Al_2O_3 (compare curves a and b, Fig. 11b). After 800°C heat treatment, the NO desorption profile of Sn5 becomes very similar to that of Al_2O_3 (compare curves a and c, Fig. 11b), suggesting that a high degree of sintering of SnO_2 and exposure of Al_2O_3 previously covered by SnO_2. For SnO_2/Al_2O_3, prepared by methods other than impregnation with $SnCl_2$, it appears that 800°C calcination is insufficient to initiate SnO_2 agglomeration as is suggested by the absence of XRD detectable peaks. The present data is insufficient to distinguish between the two possibilities, although the latter seems quite plausible.

The formation of NO_2 and its subsequent activation of the hydrocarbon reductant have been demonstrated in many catalysts to be essential initial steps in the lean NO_x process (10, 13, 17, 25). Over all SnO_2/Al_2O_3 catalysts, the C_3H_6 conversions are higher with NO_x in the feed, suggesting that NO_2 may also play a role in the hydrocarbon activation. There is significant enhancement in the low temperature NO_x conversion of Sn1 catalyst when NO_2 replaces NO in

the feed. However, it is not clear whether the improved activity takes place over the SnO_2 or Al_2O_3 sites. This is because pure Al_2O_3 is very active in promoting the reduction of NO_2 to N_2 by C_3H_6 (1, 7), and that on low Sn loading catalysts the concentration of exposed Al_2O_3 active sites may be significant. Over Sn5 and Sn10 catalysts, both the propene and NO_x conversions show little dependence on the nature of NO_x in the feed (NO or NO_2) and this indicates that either the oxidation of NO to NO_2 or the reduction of NO_2 to NO is very rapid over these catalysts. Table 1 shows that in the NO_2 reduction experiments, although the NO_2/NO ratios in the exit gas are below the equilibrium values at all temperatures, the NO_2 concentrations are not negligible. Indeed, for Sn10 at 400°C, the NO_2 concentration is comparable to NO, and yet the both the NO_x and hydrocarbon conversions are the same as when NO is in the feed (compare Figs. 1 and 2 and see Fig. 3). Thus, the formation of adsorbed NO_2 must be facile over these catalysts. The adsorbed NO_2 does not desorb readily and poisons the active site unless it is removed by a reductant. The strong adsorption of NO_2 is reflected in the poor activities observed in the NO oxidation experiments (Fig. 4). The facile oxidation of NO to adsorbed NO_2 is consistent with the model of easily reducible amorphous SnO_2 (the fraction that reduces below 450°C) being the active phase. The ease of reduction of Sn^{4+} to Sn^{2+} would facilitate the process of O_2 activation.

The lean NO_x catalysts reported in the literature can roughly be categorized into two types. The first class of catalysts are generally bulk oxides (although they can be supported to increase the surface areas) and the cations of the active phase cannot easily undergo redox reactions. Typical examples are Al_2O_3 and Ga_2O_3 (26, 27). These catalysts are generally very poor in activating hydrocarbon with oxygen alone but the hydrocarbon conversions can be improved significantly by the addition of NO_x. The substitution of NO_2 for NO in the reaction feed has great positive impact on both the activity and competitiveness factor (27, 28). In a NO feed, NO conversion increases with increasing with O_2 concentration (26). These behaviors are distinct from the second class of lean NO_x catalysts. In the latter class, the active center is composed of a reducible cation and examples are Cu-ZSM-5 and Cu-ZrO_2. High NO_x conversions are favored by low metal loadings and presumably high dispersion of the active cation (1, 7, 29, 30). The NO_x reduction activities of these catalysts are sensitive to the oxygen concentration in the feed. Beyond 1% or 2% O_2 in the feed, the NO_x conversions decrease with increasing O_2 concentration (29, 31). There is little or no dependence of the N_2 yield on the nature of NO_x as NO oxidation is very facile over these catalysts (15, 17). In all aspects, SnO_2/Al_2O_3 behaves like the latter class of lean NO_x catalysts except for the sensitivity to metal dispersion and high O_2 concentration (3). In these two aspects, SnO_2/Al_2O_3 resembles those catalysts that contain non-reducible cations. Thus SnO_2/Al_2O_3 appears to be a unique kind of lean NO_x catalysts.

V. CONCLUSIONS

SnO_2/Al_2O_3 is one of the most active lean NO_x catalysts reported in the literature. Unlike many other lean NO_x catalysts, the catalytic properties depend very weakly on metal loadings. Physical characterization indicates a wide range of oxo–tin species on these catalysts, which may be related to the dispersion of Sn. Thus, the dispersion of Sn may not have a strong influence over the competitiveness factor. The active site appears to be easily reducible, amorphous SnO_2. Large crystallites of SnO_2 may not be important simply because of their low surface areas. The catalytic performance of SnO_2/Al_2O_3 is favored by the presence of a high concentration of oxygen and this aligns it with the class of lean NO_x catalyst where the active cation is non-reducible. However, the indifference of the catalytic performance to the nature of NO_x and the ease of reducibility of a significant population of the oxo–tin species in the H_2 TPR experiments are properties usually characteristic of catalysts where the active center is reducible. Thus the properties of SnO_2/Al_2O_3 catalysts straddle between the two classes of lean NO_x catalysts and this may account for the very high NO_x activity observed over these catalysts.

ACKNOWLEDGMENT

Support by the U.S. Department of Energy, Basic Energy Sciences, and General Motor Corporation is gratefully acknowledged.

REFERENCES

1. Yang, J., Kung, M. C., Sachtler, W. M. H., and Kung, H. H., *J. Catal.* **172**, 178 (1997).
2. Teraoka, Y., Harada, T., Iwasaki, T., Ikeda, T., and Kagawa, S., *Chem. Lett.* 773 (1993).
3. Kung, M. C., Park, P. W., Kim, D.-W., and Kung, H. H., *J. Catal.* **181**, 1 (1999).
4. Miyadera, T., and Yoshida, K., *Chem. Lett.* 1483–1486 (1993).
5. Maunula, T., Kintaichi, Inaba, M., Haneda, M., Sato, K., and Hamada, H., *Appl. Catal. B: Environ.* **15**, 291 (1998).
6. Hirao, Y., Yokoyama, C., and Misono, M., *Chem. Commun.* 597 (1996).
7. Bethke, K. A., and Kung, H. H., *J. Catal.* **172**, 93 (1997).
8. Feng, X., and Hall, W. K., *J. Catal.* **166**, 368 (1997).
9. Sachtler, W. M. H., and Chen, H.-Y., *Catal. Today* **42**, 73 (1998).
10. Sasaki, M., Hamada, H., Kintaichi, and Takehiko, I., *Catal. Lett.* **15**, 297 (1992).
11. Petunchi, J. O., and Hall, W. K., *Appl. Catal. B* **2**, L17 (1993).
12. Yokoyama, C., and Misono, M., *J. Catal.* **150**, 9 (1994).
13. Aylor, A. W., Lobree, L. J., Reimer, J. A., and Bell, A. T., *Stud. Surf. Sci. Catal. A* **101**, 661 (1996).
14. Li, Y. J., and Armor, J. N., *J. Catal.* **151**, 376 (1994).
15. Chajar, Z., Primet, M., Praliaud, H., Chevrier, M., Gauthier, C., and Mathis, F., *Catal. Lett.* **28**, 33 (1994).
16. Maeda, K., Mizukami, F., Newa, S., Toba, M., Watanabe, M., and Masuda, K., *J. Chem. Soc., Faraday Trans.* **88**(1), 97 (1992).

17. Bethke, K. A., Li, C., Kung, M. C., Yang, B., and Kung, H. H., *Catal. Lett.* **31**, 287 (1995).
18. Shelef, M., Montreuil, and Jen, H. W., *Catal. Lett.* **26**, 277 (1994).
19. Lau, C. L., and Wertheim, G. K., *J. Vac. Sci. Technol.* **15**, 622 (1978).
20. Themlin, J. M., Chtaib, M., Henrard, L., Lambin, P., Darville, J., and Gilles, J.-M., *Phys. Rev. B* **46**, 2460 (1992).
21. Li, Y., and Armor, J. N., *Appl. Catal. B* **2**, 23 (1993).
22. Campa, M. C., De Rossi, S., Ferraris, and Indovina, V., *Appl. Catal. B: Environ.* **8**, 315 (1996).
23. Stakheev, A. Yu., Lee, C. W., Park, S. J., and Chong, P. J., *Catal. Lett.* **38**, 271 (1996).
24. Li, Y., and Armor, J. N., *Appl. Catal. B* **3**, L1 (1993).
25. Lukyanov, D. B., Sill, G., d'Itri, J. L., and Hall, W. K., *J. Catal.* **153**, 265 (1995).
26. Hamada, H., Kintaichi, Y., Sasaki, M., and Takehiko, I., *Appl. Catal.* **70**, L15 (1991).
27. Kung, M., Bethke, K., Alt, D., Yang, B., and Kung, H., *ACS Symp. Ser.* **587**, 96 (1995).
28. Kung, M. C., Lee, J.-H., Chu-Kung, A., and Kung, H. H., *Stud. Surf. Sci. Catal. A* **101**, 701 (1996).
29. Bethke, K. A., Alt, D., and Kung, M. C., *Catal. Lett.* **25**, 37 (1994).
30. Torikai, Y., Yahiro, H., Mizuno, N., and Iwamoto, M., *Catal. Lett.* **9**, 91 (1991).
31. Iwamoto, M., Mizuno, N., and Yahiro, H., *Proc. Int. Congr. Catal.*, 10th, 1285 (1993).